ACS APPLIED MATERIALS & INTERFACES

Research Article

www.acsami.org

2-Thiopheneacetic Acid Directed Synthesis of Au Nanorosette as an SERS-Active Substrate

Hye-Seon Shin, Jin-Yeon Hong, and Seong Huh*

Department of Chemistry and Protein Research Center for Bio-Industry, Hankuk University of Foreign Studies, Yongin, 449-791, Korea

Supporting Information

ABSTRACT: Rosette-like nanoscale Au materials were simply prepared through one-pot reduction of the $AuCl_4^-$ precursor by 2-thiopheneacetic acid (2-TAA) without extra surface capping ligands at room temperature. 2-TAA underwent polymerization into polythiophene derivatives while the $AuCl_4^-$ precursor was simultaneously reduced into various Au nanostructures. In situ generated polythiophene derivatives played a significant role of surface passivation in guiding the shape of Au nanostructures. The morphology of Au nanostructures was strongly dependent on the molar ratio of 2-TAA to $AuCl_4^-$. At lower $[2\text{-TAA}]/[AuCl_4^-]$ ratios, uniform rosette-like Au microparticles consisting of 30-nm-thick Au nanoplates were observed. The Au nanoplates had either triangular prismatic or hexagonal geometry with many defects. Uniform Au nanorosettes could be easily deposited on the Si substrate by drop-casting and were subsequently used as highly active SERS substrates for the detection of methylene blue and crystal violet by Raman spectroscopy. Upon increasing the ratio of $[2\text{-TAA}]/[AuCl_4^-]$, Au nanoparticles or nanorods heavily surrounded with polythiophene polymers were obtained.

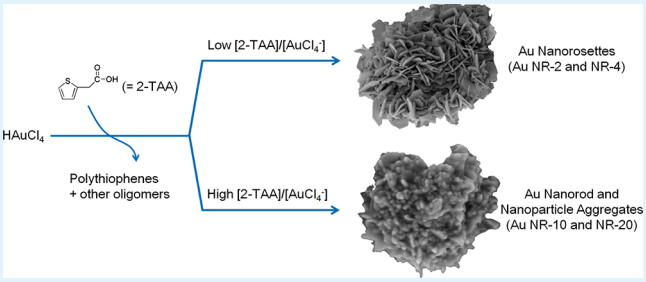

KEYWORDS: *gold nanostructure, surface-enhanced Raman scattering, methylene blue, crystal violet*

1. INTRODUCTION

Materials science research on nanoscale Au is becoming extremely popular in a wide range of technologically important areas.[1] For instance, the unique optical properties of Au nanoparticle (NP) have led to many progresses in biological sensing applications.[2] The surface-enhanced Raman scattering (SERS) effect by sharp tips or nanogap hotspots of nanoscale Au has indeed enriched the practical application potential of Au-based nanostructures.[3] The SERS-based sensing system has been considered as one of the powerful tools for signal amplification and detection since its discovery in 1974 by Fleischmann et al.[4] Not only did this system overcome the several limitations of conventional Raman scattering but it has also enabled us to open a new era of molecular detection based on spectroscopic techniques. Special architectures of metallic substrates, typically Ag,[5] Au,[6] or even sometimes Pd,[7] are required for efficient Raman signal enhancement since their values of the dielectric constant are in the appropriate range to support localized electron oscillations or localized surface plasmon resonance (LSPR). With increasing interest on the discovery of proper metal substrates for SERS-based applications, three-dimensional (3D) morphology control of metallic nanostructures to generate effective and adequate hotspots for creating strong and tunable electromagnetic field is gaining great attention.[8] We recently demonstrated that a simple reduction process of the Au precursor, $AuCl_4^-$, using a polymerizable 2-thiophene derivative led to thin Au nanoleaf materials possessing abundant nanogaps with an average dimension of 4.8 nm.[9] In this case, the employed 2-thiophenemethanol underwent oxidative polymerization in the presence of $AuCl_4^-$ during the simultaneous formation of novel Au nanoleaves. The most important concept in this seedless preparation strategy was the use of a polymerizable monomer both as a reducing agent and a shape-controlling ligand.

Here, we report a 2-thiopheneacetic acid (2-TAA)-directed fabrication of uniform rosette-like Au nanostructures with highly textured acute surfaces with high SERS activity. In this approach, we also took advantage of the bifunctional role of 2-TAA as both a reducing agent for the Au precursor and an effective surface-stabilizing agent during formation of Au nanostructures. The Au nanorosette (Au NR) species consisted of either triangular prisms or hexagonal nanoplates exhibiting evident SERS enhancement for the detection of methylene blue (MB) and crystal violet (CV). The detection limits were 10^{-9} M and 10^{-7} M, respectively.

2. EXPERIMENTAL SECTION

Preparation of Au Nanostructures. 2-TAA (30 mg, 0.211 mmol for Au NR-2; 60 mg, 0.422 mmol for Au NR-4; 150 mg, 1.055 mmol

Received: November 27, 2012
Accepted: January 21, 2013
Published: January 21, 2013

Scheme 1. Illustration of the Formation of Au Nanostructures by 2-TAA

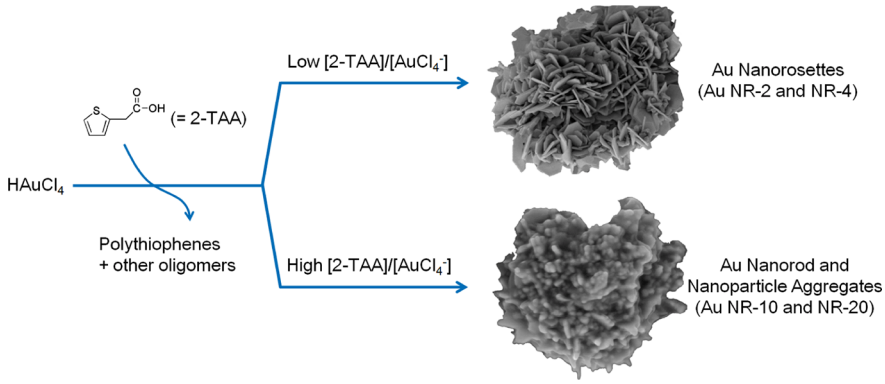

for Au NR-10; 300 mg, 2.110 mmol for Au NR-20) was completely dissolved in 10 mL of deionized water. $HAuCl_4 \cdot 3H_2O$ (40 mg, 0.102 mmol) was added to the solution, and the mixture was gently stirred for 6 h. After this, dark-green colored products were separated by centrifugation at 9000 rpm and washed with copious amounts of deionized water several times. The final solids were dried in an oven at 80 °C.

Experimental Preparation for SERS. Different amounts of Au NR-2 solids (10 mg, 30 mg, and 50 mg) were redispersed in deionized water (20 mL) and sonicated fully enough to make Au-suspended mother liquors. A drop of the suspension (30 μL) was casted on a well-polished Si wafer and dried at 80 °C for 30 min. The drop-and-dry procedure was repeated once again on the same place of the wafer. The as-prepared dye solution (30 μL) with a proper concentration was dropped on the same spot of the Au-treated Si wafer and dried in the dark under ambient conditions.

Physical Measurements. Powder X-ray diffraction patterns were recorded on a Rigaku MiniFlex (30 kV, 15 mA). FE-SEM images were recorded on a Hitachi Ultra-High-Resolution Analytical FE-SEM SU-70 (5 kV). The water suspension of the sample was dropped and dried on the Cu grid supported by a holey carbon film for TEM measurement, in which a JEOL JEM-3000F (300 kV) equipped with an EDAX for EDS spectrum was used. XPS data were collected on a Kα monochromated high-performance XPS spectrometer (Thermo VG, UK). The X-ray source was a monochromated Al Kα line ($h\nu$ = 1486.6 eV), and the X-ray power was 12 kV and 3 mA. The pass energy of the analyzer for high-resolution spectrum was fixed at 50 eV. The sampling area was 400 μm in diameter. The binding energies were referenced to 284.8 eV (C 1s peak for C−C bonds). Micro-Raman measurements were performed in backscattering geometry with a Horiba Jobin Yvon LabRam HR system fitted with a liquid-nitrogen cooled CCD multichannel detector. Spectra were collected under ambient conditions using the 633 nm line of a He−Ne laser. Au NR-2 drop-casted on the Si wafer was exposed with a laser power of 0.05 mW for an acquisition time of 30 s with an area of 1 μm in diameter.

3. RESULTS AND DISCUSSION

The Au precursor, $AuCl_4^-$, was simply reduced by various concentrations of 2-TAA in an aqueous solution at room temperature with constant stirring. The molar ratios of $[AuCl_4^-]$:[2-TAA] were 1:2 (Au NR-2), 1:4 (Au NR-4), 1:10 (Au NR-10), and 1:20 (Au NR-20) (Au NR-*n* indicates the sample prepared by an *n*-fold excess amount of 2-TAA relative to the $AuCl_4^-$ precursor). The retrieved solid products from the reactions were investigated by scanning electron microscopy (SEM) to determine the shape of Au nanostructures, as shown in Figure 1. There were mainly three different shapes of Au nanostructures. At lower $[2\text{-TAA}]/[AuCl_4^-]$ conditions, that is, Au NR-2 and Au NR-4, rosette-like spherical microparticles consisting of thin Au nanoplates were observed. The thickness of each Au nanoplate was about 30 nm. On the contrary,

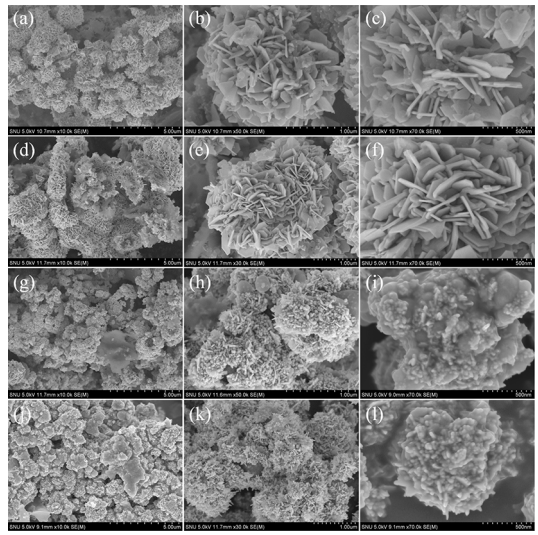

Figure 1. FE-SEM images of the Au nanostructures on different magnifications. (a−c) Au NR-2, (d−f) Au NR-4, (g−i) Au NR-10, and (j−l) Au NR-20.

relatively higher $[2\text{-TAA}]/[AuCl_4^-]$ conditions, i.e., Au NR-10 and Au NR-20, generated Au nanoparticles (NPs) or nanorods that were completely surrounded with excess in situ generated polythiophene polymers. The shape of the Au nanostructure was therefore strongly dependent on the ratio of $[2\text{-TAA}]/[AuCl_4^-]$. When higher than 10-fold excess amount of 2-TAA with respect to the Au precursor was used, the reaction proceeded very quickly, generating a large amount of polymers. These rapidly grown polymers seemed to effectively encapsulate the simultaneously formed Au NPs or nanorods.[9] Hence, the kinetics controlled by different concentrations of 2-TAA changed the shape of final Au nanostructures. These results clearly suggest that the role of 2-TAA both as a reducing agent and a surface-stabilizing ligand is extremely critical in the shape control of Au nanostructures.

The Au nanostructures were further analyzed by transmission electron microscopy (TEM) to characterize the detailed shape of Au nanostructures as depicted in Figure 2. High-resolution TEM (HR-TEM) investigation was also performed to determine the crystalline nature of the Au nanostructures. Both Au NR-2 and Au NR-4 were revealed to be neither in the form of a perfect hexagonal plate nor in the form of a triangular prism which is frequently observed for thin Au nanoplates.[10] Most of the nanoplates contained defects as depicted in panels b, d, and e in Figure 2. Representative hexagon and triangular

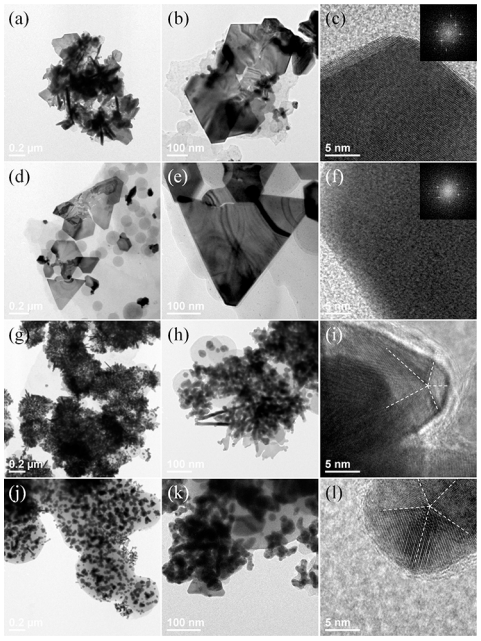

Figure 2. TEM images of the Au nanostructures. (a–c) Au NR-2, (d–f) Au NR-4, (g–i) Au NR-10, and (j–l) Au NR-20. White lines in (i) and (l) indicate the pentagonally twinned lattices.

prisms with defects are also depicted in Figure 3. The defects were located either at the center or the edge of the nanoplate.

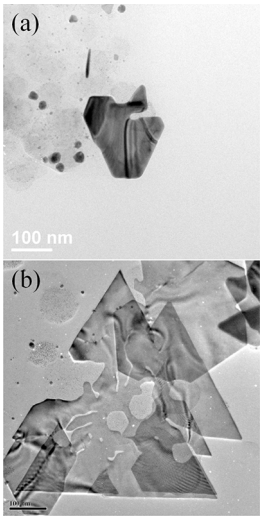

Figure 3. TEM images of (a) the defected hexagonal and (b) triangular prismatic nanostructures of Au NR-2.

We previously observed dendritic nanostructures in the early stage of Au nanoleaf formation.[9] In fact, dendritic nanostructures were frequently observed during formation of well-shaped noble metal nanocrystals via the seeded-growth method.[11] Thus, dendritic nanostructures are considered as key intermediate structures during metallic nanocrystal formation. Even though we employed the seedless preparation method as our current synthetic approach, dendritic nanostructures can also be considered as an intermediate of perfect hexagonal or triangular prismatic nanoplates. Defected nanoplates may result from incomplete formation of hexagonal or triangular prismatic nanoplate geometry due to in situ generated polythiophene polymers rather than the etching mechanism of preformed hexagon or triangular prism.[12] These defects may have beneficial effects on SERS-based sensing due to the generation of sharp tips or nanogaps. Each thin Au nanoplate was determined as the crystalline Au material with exposed top and bottom surfaces of the Au(111) plane, the most stable crystalline facet for face-centered cubic (fcc) metals.[13] HR-TEM images depicted in panels c and f in Figure 2 clearly demonstrate the crystalline plane of fcc Au(111).

Both Au NR-10 and Au NR-20 exhibited nanoparticles that were completely embedded in the polymers. Interestingly, HR-TEM images revealed the nanoparticles or nanorods with a penta-twinned corner structure.[14]

These results suggest that a relatively large amount of in situ generated polythiophenes in high [2-TAA]/[$AuCl_4^-$] conditions effectively prevents further growth of Au NPs by passivation of Au{100} facets.

Yang and Huang also reported Au nanostructures by using 3-thiopheneacetic acid (3-TAA) as a sole reducing agent.[15] 3-TAA can polymerize through 2- and 5-positions of the thiophene ring because these positions are available during the redox process. This polymerization is usually faster than the polymerization of 2-TAA which may occur after the removal of the 2-positioned functional group. Faster polymerization usually leads to small Au NPs.[9,15] For 2-TAA, another possibility is that the polymerization may occur through 3-positioned carbon atom instead of 2-positioned carbon atom. We believe that our preparation method is clearly different from the procedure published in the literature.[15] In short, we maintained a very low stirring speed (60 rpm) during the preparation of Au nanostructures by 2-TAA and which might result in aggregated defected nanoplates, i.e., rosette-like structure, instead of tiny Au NPs, perfect hexagonal plates, or perfect triangular prisms as reported by Yang and Huang.[15]

Powder X-ray diffraction (PXRD) patterns were investigated for the determination of bulk crystalline phase. The well-resolved eight diffraction peaks were observable for Au NR-2 at 2θ = 38.16, 44.36, 64.64, 77.62, 81.68, 98.34, 111.04, and 115.22°, which were assigned to the typical fcc Au crystal planes of (111), (200), (220), (311), (222), (400), (331), and (420), respectively, as shown in Figure 4.[16] From the intensity ratios of the {111} plane to other diffraction peaks, it is noteworthy that there were more high index facets for Au NR-2 compared with the bulk Au sample. In particular, I_{220}/I_{111} (= 0.42), I_{311}/I_{111} (= 0.50), and I_{222}/I_{111} (= 0.18) exhibited larger values than the corresponding values of bulk Au, 0.32, 0.36, and

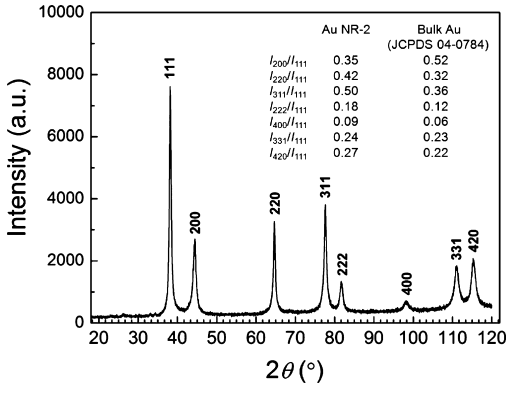

Figure 4. PXRD pattern of Au NR-2.

dx.doi.org/10.1021/am302865b | ACS Appl. Mater. Interfaces 2013, 5, 1429–1435

0.12, respectively (JCPDS No. 04-0784). The lattice parameter and the *d*-spacing value calculated from the diffraction pattern of (111) plane were 4.082 Å and 2.357 Å, respectively, which were in good agreement with HR-TEM observation and reference PXRD data (JCPDS No. 04-0784, a = 4.078 Å, d_{111} = 2.355 Å).

The Fourier-transform infrared (FT-IR) spectrum was taken for Au NR-2 as depicted in Figure 5b. Interestingly, the carboxy

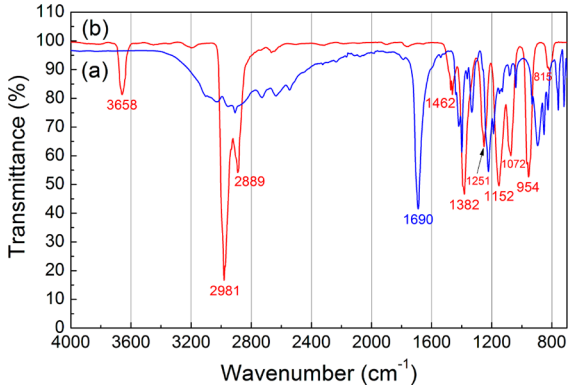

Figure 5. FT-IR spectra of (a) neat 2-TAA and (b) Au NR-2.

group absorption band of neat 2-TAA at 1690 cm^{-1} (Figure 5a) virtually disappeared after the formation of Au NR-2. We propose that decarboxylation of 2-TAA might have occurred during the reaction because the reaction mixture was acidic due to the Au precursor, $HAuCl_4$. Two strong absorption bands at 2981 cm^{-1} and 2889 cm^{-1} corresponded to the methylene moieties of the resultant polythiophene polymers. The C═C and C—S stretching bands and ═C−H out of plane mode were observed at 1462, 1072, and 815 cm^{-1}, respectively. A new band observed at 3658 cm^{-1} was due to residual water.[17]

A series of time-dependent UV/vis absorption spectra during the formation of Au NR-2 were recorded throughout the reduction process as given in Figure 6. As depicted in Figure 6a, two distinct surface plasmon resonance (SPR) absorption bands appeared around 578 and 740 nm at the beginning of the reduction process and gradually developed throughout the broad range of wavelengths. The former band can be attributed to the transverse SPR band and the latter to the longitudinal SPR band.[18] Even though plasmonic resonance absorption of tiny spherical Au NP (9−22 nm) usually occurs at 520 nm,[18] the red-shifted transverse SPR band centered at 578 nm for Au NR-2 is reasonably rationalized since SPR absorption is strongly governed by the size and the 3D structure of the particle.[19] Becasue SPR is a consequence of the superposition of individual NPs, the appearance of a broad red-shifted transverse SPR band is taken into account by agglomeration of NPs or variation in NP size, and these preferential broadening and shifts also indicate substantial changes in NP morphology during the reduction period. The appearance of the SPR bands with a short evolution time implies that the reduction is a rather fast process and its baseline shift seems to be the result of the scattering effect in solution. After 195 min, however, both transverse and longitudinal SPR bands almost completely disappeared as shown in Figure 6c.

The detailed elemental states of Au NR-2 were examined by X-ray photoelectron spectroscopy (XPS). The survey spectrum in Figure 7a shows the binding energies of C 1s, S 2s, S 2p, Au

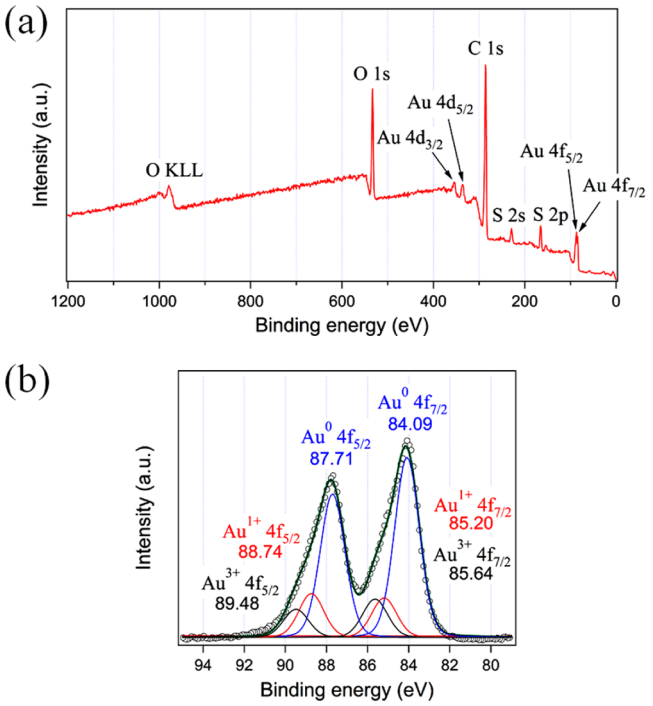

Figure 7. (a) XPS survey spectrum of Au NR-2 and (b) its high-resolution Au 4f XPS spectrum.

4d, and Au 4f. Therefore, the thiophene moieties and Au were found by XPS analysis. Each binding energy was calibrated with the C 1s peak at 284.8 eV as a reference value.[20] High-resolution Au 4f XPS spectrum is depicted in Figure 7b.

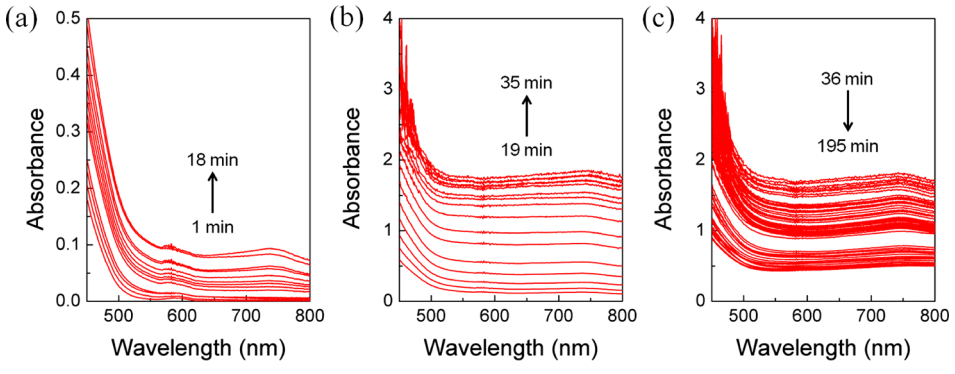

Figure 6. Time-dependent UV/vis spectra taken during formation of Au NR-2.

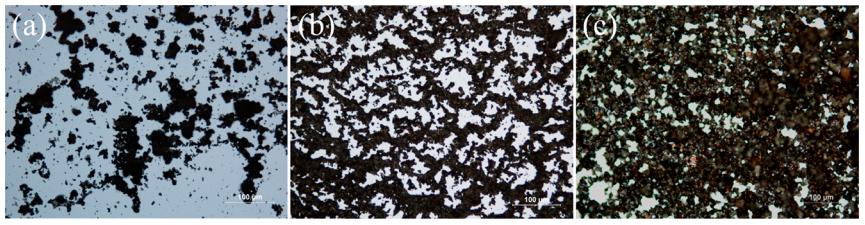

Figure 8. Optical micrographs of the dried Au NR-2 sample drop-casted on Si wafers for SERS measurements. (a) 10 mg, (b) 30 mg, and (c) 50 mg Au NR-2 in each mother liquor.

Ionization of Au 4f exhibited a doublet of $4f_{7/2}$ and $4f_{5/2}$ at 84.09 and 87.71 eV, respectively, for metallic Au^0,[21] a doublet at 85.20 and 88.74 eV for oxidized Au^{1+},[22] and another doublet at 85.64 and 89.48 eV for oxidized Au^{3+} with typical spin−orbit splitting of 3.7 eV.[23] The latter two binding energies demonstrate the partially oxidized surface of Au NR-2. The corresponding area ratio of Au^o:Au^{1+}:Au^{3+} was 68%:14%:18%.

Au nanostructures with sharp tips and nanogaps are often considered as superior SERS substrates.[3] Therefore, we investigated the potential of Au NR-2 as an SERS-active substrate using two important biological staining agents, methylene blue (MB) and crystal violet (CV) which have been reported to give good quality Raman spectra, as probe molecules.[9,24] Au NR-2 could be uniformly deposited on a Si wafer by drop-casting. Optical microscopic images of the uniformly distributed Au NR-2 solids on Si wafers are shown in Figure 8. Depending on the amount of Au NR-2 in a mother liquor, the density of Au NR-2 on a Si wafer could be controlled.

A set of Raman spectra obtained for different concentrations of MB and CV by using Au NR-2 (30 mg in a mother liquor) are depicted Figure 9. As the concentration of MB decreases, the intensities of the bands at 1623 cm^{-1} and 1395 cm^{-1} corresponding to aromatic C−C ring stretching and N−C symmetrical phenyl vibration stretching also decrease, but the signal of the 10^{-9} M sample is still discernible (Figure 9a). In the spectra of CV in Figure 9b, the characteristic signals of 1617 cm^{-1} and 1175 cm^{-1} ascribed to the C−C aromatic ring skeletal vibration and C−H in-plane bending vibrations are clearly distinguished from the background signal down to the concentration of 10^{-7} M. No significant signals of MB and CV were detected on the commercial flat gold surface (layer thickness 100 Å, Aldrich catalog no. 643203) even with the concentration of 10^{-5} M. The SERS enhancement factors (EFs) for MB and CV based on the detection limits were estimated to be about 2.6×10^8 and 8.8×10^5, respectively.[9] Although there are no available theoretical comparison data of MB and CV for SERS on the Au surface, it is thought that the larger size of CV molecule leads to lower density on the metallic surfaces and may be partly responsible for its relatively lower sensitivity than that of MB. When different amounts of Au NR-2 samples on a Si wafer were employed for the same measurements, Au NR-2 concentration-dependent SERS activity was observed. Both smaller and larger amounts of Au NR-2 on Si wafer substrates compared with the substrate prepared from 30 mg Au NR-2 mother liquor exhibited decreased signals as depicted in Figure 10. The detection limits of MB decreased to 10^{-8} M and 10^{-7} M, respectively. Therefore, optimal concentration of the deposited Au NR-2 is also important for an enhanced detection.

The rosette-like Au nanostructures with highly textured morphology indeed produced high SERS activity for the detection of MB and CV because the probe molecules could be effectively deposited between the acute triangular surfaces or defects where strong Raman enhancements were generated. The SEM images and high SERS EFs obviously confirm that the sharp apexes of the defected Au hexagonal plates and Au prisms of the rosette-like Au morphology are clearly the hotspots for the enhanced electric field generation.

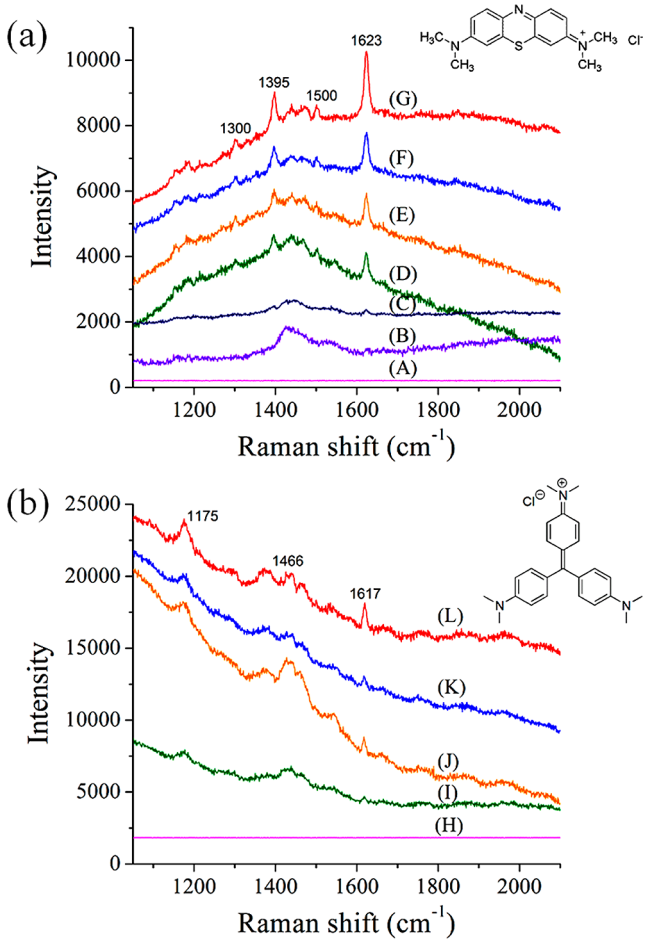

Figure 9. Concentration-dependent Raman spectra of (a) MB and (b) CV: (A) the MB solution (1×10^{-5} M) on a flat Au coated glass, MB solutions on the Au NR-2 sample (30 mg in a mother liquor) on a Si wafer (B) 1×10^{-9} M, (C) 1×10^{-8} M, (D) 1×10^{-7} M, (E) 1×10^{-6} M, (F) 1×10^{-5} M, and (G) 1×10^{-4} M. (H) The CV solution (1×10^{-5} M) on flat Au coated glass, and CV solutions on the Au NR-2 sample on a Si wafer (I) 1×10^{-7} M, (J) 1×10^{-6} M, (K) 1×10^{-5} M, and (L) 1×10^{-4} M. The chemical structures of MB and CV are indicated together.

dx.doi.org/10.1021/am302865b | ACS Appl. Mater. Interfaces 2013, 5, 1429−1435

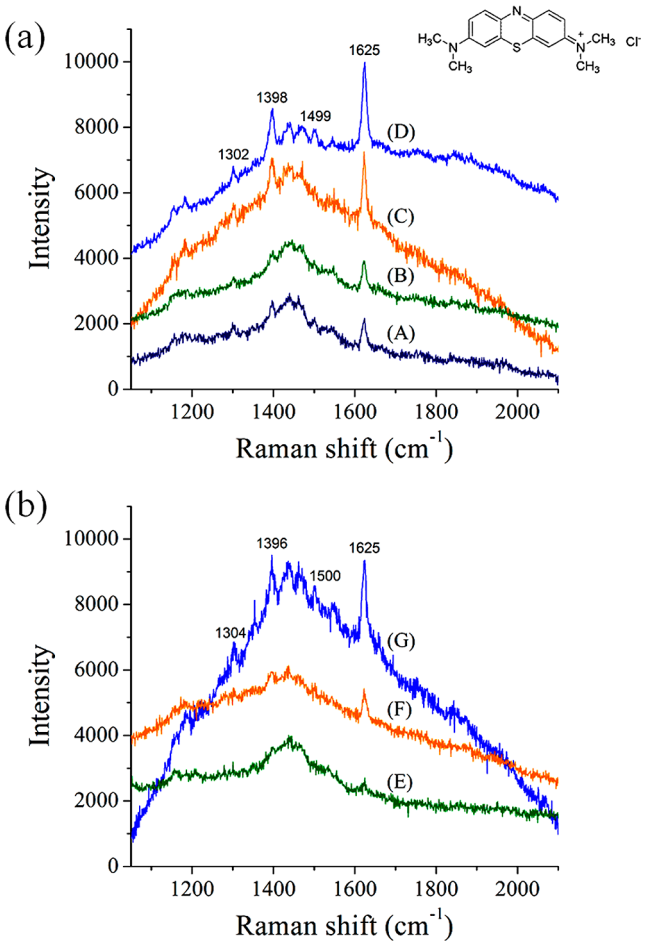

Figure 10. Concentration-dependent Raman spectra of MB: (a) Au NR-2 (10 mg in a mother liquor) and (b) Au NR-2 (50 mg in a mother liquor) on a Si wafer: MB solutions on the Au NR-2 sample on a Si wafer (A) 1×10^{-8} M, (B) 1×10^{-7} M, (C) 1×10^{-6} M, (D) 1×10^{-5} M, (E) 1×10^{-7} M, (F) 1×10^{-6} M, and (G) 1×10^{-5} M. The chemical structure of MB is indicated.

4. CONCLUSIONS

We developed a facile preparation method for SERS-active rosette-like Au nanostructures under ambient conditions by taking advantages of the dual role of 2-TAA both as a reducing agent and a surface stabilizing ligand. Polymerization of 2-TAA was observed during the redox process, and the simultaneously generated polythiophene derivatives functioned as good surface capping ligands. At relatively low [2-TAA]/[$AuCl_4^-$] conditions, rosette-like Au nanostructures were favored while higher [2-TAA]/[$AuCl_4^-$] conditions yielded a mixture of Au NPs or nanorods fully encapsulated by the in situ generated polythiophene polymers. Rosette-like Au nanostructures are good SERS substrates for MB and CV with the respective SERS EFs of 2.6×10^8 and 8.8×10^5. Despite various previous examples of SERS-active Au nanostrucutres,[25−31] our current one-pot reduction method of $AuCl_4^-$ by 2-TAA is very simple, efficient, and highly reproducible. We envision that this new synthetic approach for Au nanostructures will provide new opportunities for the efficient preparation of other functional metallic nanostructures.

■ ASSOCIATED CONTENT

Ⓢ Supporting Information

SERS enhancement factor calculation. This material is available free of charge via the Internet at http://pubs.acs.org.

■ AUTHOR INFORMATION

Corresponding Author

*E-mail: shuh@hufs.ac.kr.

Author Contributions

The manuscript was written through contributions of all authors.

Notes

The authors declare no competing financial interest.

■ ACKNOWLEDGMENTS

This work was supported by the Basic Science Research Program through the National Research Foundation of Korea (NRF) funded by the Ministry of Education, Science and Technology (2010-0010096) and the Gyeonggi Regional Research Center (GRRC) program of Gyeonggi province (GRRC-HUFS-2012-A01).

■ ABBREVIATIONS

NR, nanorosette; NP, nanoparticle; 2-TAA, 2-thiopheneacetic acid; FT-IR, Fourier transform infrared; TEM, transmission electron microscopy; SEM, scanning electron microscopy; PXRD, powder X-ray diffraction; XPS, X-ray photoelectron spectroscopy; SERS, surface-enhanced Raman scattering; MB, methylene blue; CV, crystal violet

■ REFERENCES

(1) Dreaden, E. C.; Alkilany, A. M.; Huang, X.; Murphy, C. J.; El-Sayed, M. A. *Chem. Soc. Rev.* **2012**, *41*, 2740−2779.
(2) Saha, K.; Agasti, S. S.; Kim, C.; Li, X.; Rotello, V. M. *Chem. Rev.* **2012**, *112*, 2739−2779.
(3) Walker, D. A.; Browne, K. P.; Kowalczyk, B.; Grzybowski, B. A. *Angew. Chem., Int. Ed.* **2010**, *49*, 6760−6763.
(4) Fleischmann, M.; Hendra, P. J.; McQuillan, A. J. *Chem. Phys. Lett.* **1974**, *26*, 163−166.
(5) Gutés, A.; Carraro, C.; Maboudian, R. *J. Am. Chem. Soc.* **2010**, *132*, 1476−1477.
(6) He, J.; Zhang, P.; Gong, J.; Nie, Z. *Chem. Commun.* **2012**, *48*, 7344−7346.
(7) Xiong, Y.; McLellan, J. M.; Chen, J.; Yin, Y.; Li, Z.-Y.; Xia, Y. *J. Am. Chem. Soc.* **2005**, *127*, 17118−17127.
(8) Angelomé, P. C.; Mezerji, H. H.; Goris, B.; Pastoriza-Santos, I.; Perez-Juste, J.; Bals, S.; Liz-Marzán, L. M. *Chem. Mater.* **2012**, *24*, 1393−1399.
(9) Hong, J.-H.; Hwang, Y.-K.; Hong, J.-Y.; Kim, H.-J.; Kim, S.-J.; Won, Y. S.; Huh, S. *Chem. Commun.* **2011**, *47*, 6963−6965.
(10) Shankar, S. S.; Rai, A.; Ankamwar, B.; Singh, A.; Ahmad, A.; Sastry, M. *Nat. Mater.* **2004**, *3*, 482−488.
(11) Huang, M. H.; Lin, P.-H. *Adv. Funct. Mater.* **2012**, *22*, 14−24.
(12) Soejima, T.; Kimizuka, N. *J. Am. Chem. Soc.* **2009**, *131*, 14407.
(13) Zhang, Y.; Wen, Y.-H.; Zhu, Z.-Z.; Sun, S.-G. *J. Phys. Chem. C* **2010**, *114*, 18841−18846.
(14) Murphy, C. J.; Sau, T. K.; Gole, A. M.; Orendorff, C. J.; Gao, J.; Gou, L.; Hunyadi, S. E.; Li, T. *J. Phys. Chem. B* **2005**, *109*, 13857−13870.
(15) Huang, H.; Yang, X. *Colloids Surf., A* **2005**, *255*, 11−17.
(16) Hakamada, M.; Mabuchi, M. *Nano Lett.* **2006**, *6*, 882−885.
(17) Praprotnik, M.; Janežic, D.; Mavri, J. *J. Phys. Chem. A* **2004**, *108*, 11056−11062.
(18) Ghosh, S. K.; Pal, T. *Chem. Rev.* **2007**, *107*, 4797−4862.

(19) Sun, X.; Dong, S.; Wang, E. *Angew. Chem., Int. Ed.* **2004**, *43*, 6360.
(20) Pijpers, A. P.; Meier, R. J. *Chem. Soc. Rev.* **1999**, *28*, 233−238.
(21) Wang, Z.; Zhang, Q.; Kuehner, D.; Ivaska, A.; Niu, L. *Green Chem.* **2008**, *10*, 907−909.
(22) Wei, H.; Li, B.; Du, Y.; Dong, S.; Wang, E. *Chem. Mater.* **2007**, *19*, 2987−2993.
(23) Park, E. D.; Lee, J. S. *J. Catal.* **1999**, *186*, 1−11.
(24) Yap, F. L.; Thoniyot, P.; Krishnan, S.; Krishnamoorthy, S. *ACS Nano* **2012**, *6*, 2056−2070.
(25) Lin, T.-H.; Lin, C.-W.; Liu, H.-H.; Sheu, J.-T.; Hung, W.-H. *Chem. Commun.* **2011**, *47*, 2044−2046.
(26) Mai, F.-D.; Hsu, T.-C.; Liu, Y.-C.; Yang, K.-H.; Chen, B.-C. *Chem. Commun.* **2011**, *47*, 2958−2960.
(27) Yang, M.; Alvarez-Puebla, R.; Kim, H.-S.; Aldeanueva-Potel, P.; Liz-Marzán, L. M.; Kotov, N. A. *Nano Lett.* **2010**, *10*, 4013−4019.
(28) Su, Y.; He, Q.; Yan, X.; Fei, J.; Cui, Y.; Li, J. *Chem.−Eur. J.* **2011**, *17*, 3370−3375.
(29) Bai, X.; Zheng, L. *Cryst. Growth Des.* **2010**, *10*, 4701−4705.
(30) Demeritte, T.; Kanchanapally, R.; Fan, Z.; Singh, A. K.; Senapati, D.; Dubey, M.; Zakar, E.; Ray, P. C. *Analyst* **2012**, *137*, 5041−5045.
(31) Guerrero-Martínez, A.; Barbosa, S.; Pastoriza-Santos, I.; Liz-Marzán, L. M. *Curr. Opin. Colloid Interface Sci.* **2011**, *16*, 118−127.